Final Report: Mach Zander interferometer

NACHIKET KULKARNI[1]

[1]*KLA Corporation, Milpitas, CA*
**kulknachiket@gmail.com*

Abstract:

1. Introduction

Mach-Zander interferometer (MZI) is an optical device that splits the beam of light to two paths and recombine them to observe interference patterns, providing a precise measurement of the phase shifts and other optical properties. Mach-Zander interferometers are widely used in optical testing, quantum mechanics, telecommunications, sensors, telecommunication, optical modulators, optical switches, etc. In this proposal, we design and simulate different structures of MZI to extract the effects due to change in optical path length, change in polarization and change in waveguide widths.

2. Theory

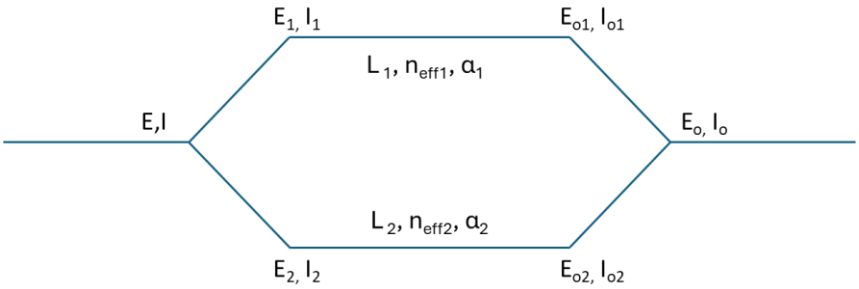

Figure 1: Typical layout of Mach-Zander interferometer

Consider a MZI system as shown in Figure 1. A typical MZI would consist of Y-splitter, waveguides, and a Y-combiner. Assume the incident electric field is E and the intensity is I, the electric field is split into two components by the splitter, namely E_1 and E_2. Assuming the Y-splitter splits the intensity into two equal components, the intensity at each branch after splitting would be I/2. The electric field at each branch would be given by:

$$E_1 = E_2 = \frac{E}{\sqrt{2}} \tag{1}$$

Assume that the electric field E_1 propagates through a waveguide whose length is L_1, effective refractive index is n_{eff1} and loss is α_1. Similarly, electric field E_2 propagates through a waveguide whose length is L_2, effective refractive index is n_{eff2} and loss is α_2. If the output electric field is E_{o1} and E_{o2}, then E_{o1} and E_{o2} are given by:

$$E_{o1} = E_1 e^{-j\beta_1 L_1 - \frac{\alpha_1 L_1}{2}}$$
$$E_{o2} = E_2 e^{-j\beta_2 L_2 - \frac{\alpha_2 L_2}{2}} \tag{2}$$

Where $\beta_{1,2} = \frac{2\Pi}{\lambda}$, λ is the wavelength of the beam.

Following the two waveguides is a Y-combiner. The effective output electric field E_o is given by:

$$E_o = \frac{E_{o1}+E_{o2}}{\sqrt{2}} \tag{3}$$

Depending on the path difference between the two waveguides, MZI can be classified as balanced MZI and unbalanced MZI. In the former configuration, the optical path length between the two waveguides is equal, while in the latter configuration the path difference between the two waveguides is unequal. Combining equations 1, 2 and 3, a direct relation between input and output electric field can be computed.

$$E_o = \frac{Ee^{-j\beta_1 L_1 - \frac{\alpha_1 L_1}{2}} + Ee^{-j\beta_2 L_2 - \frac{\alpha_2 L_2}{2}}}{2}$$

The intensity of light at the output is given by the squaring the amplitude of the electric field. Equation 4 represents a generalized equation of electric field at the output of an unbalanced MZI.

$$I_o = E_o E_o{}^* = \frac{Ee^{-j\beta_1 L_1 - \frac{\alpha_1 L_1}{2}} + Ee^{-j\beta_2 L_2 - \frac{\alpha_2 L_2}{2}}}{2} * \frac{Ee^{j\beta_1 L_1 - \frac{\alpha_1 L_1}{2}} + Ee^{j\beta_2 L_2 - \frac{\alpha_2 L_2}{2}}}{2} \tag{4}$$

Solving equation 4, output intensity I_o is given by equation 5.

$$I_o = \frac{I}{2}(1 + cos\ (\beta \Delta L))$$

where $\Delta L = L_1 - L_2$

An important parameter of a Mach-Zander interferometer is the free spectral range (FSR), which represents the wavelength spacing between successive consecutive maxima (or minima) in the transmission spectrum. This arises due to the constructive and destructive interference from the two arms of the interferometer and is correlated to the optical path difference to the two arms. The FSR is given by.

$$FSR = \frac{\lambda^2}{\Delta L n_g(\lambda)} \tag{5}$$

where n_g is the group index of waveguide, given by $n_g(\lambda) = n_{eff}(\lambda) - \lambda \frac{dn_{eff}(\lambda)}{d\lambda}$.

3. Modelling and Simulation

3.1 *Waveguide*

We will simulate a strip waveguide of height 220nm and 500nm width. The width of the waveguide is chosen for convenience, while the height of 220nm is chosen due to its effectiveness in maintaining the optical properties and ensuring proper wave propagation. Secondly, the 220nm height is also compatible with various fabrication methods and materials used in the waveguide production, making it an industry-wide adopted standard.

The modes of the waveguide were simulated in Lumerical Mode software. Figure 2a and b show the electric field intensity of TE and TM mode in the waveguide at 1550nm. Table 1 shows the effective refractive index for different modes at 1550nm.

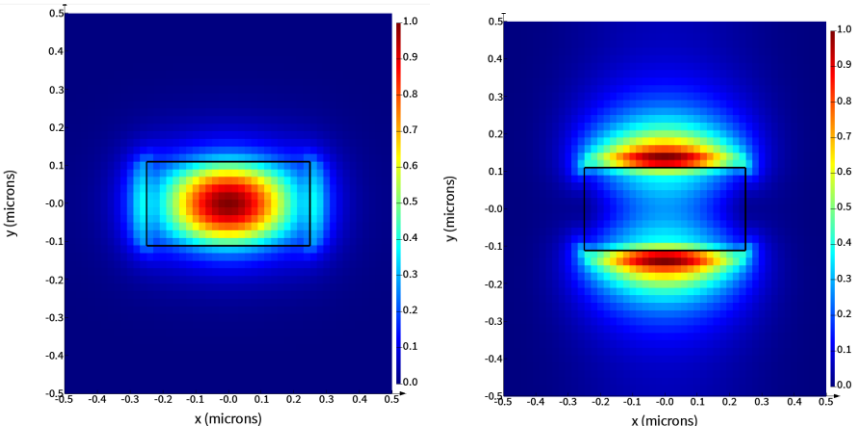

Figure 2: a) Electric intensity for the TE mode (left), b) Electric intensity for the TM mode (right)

Table 1: Effective refractive index at 1550nm for different modes (waveguide size 500nm*220nm)

Mode	Refractive Index
TE1	2.4494
TM1	1.7561
TE2	1.5254

Figure 3 A and B shows the variation of effective index and group index with wavelength. This was simulated by frequency sweep in Lumerical mode between 1.55um to 1.6um wavelength.

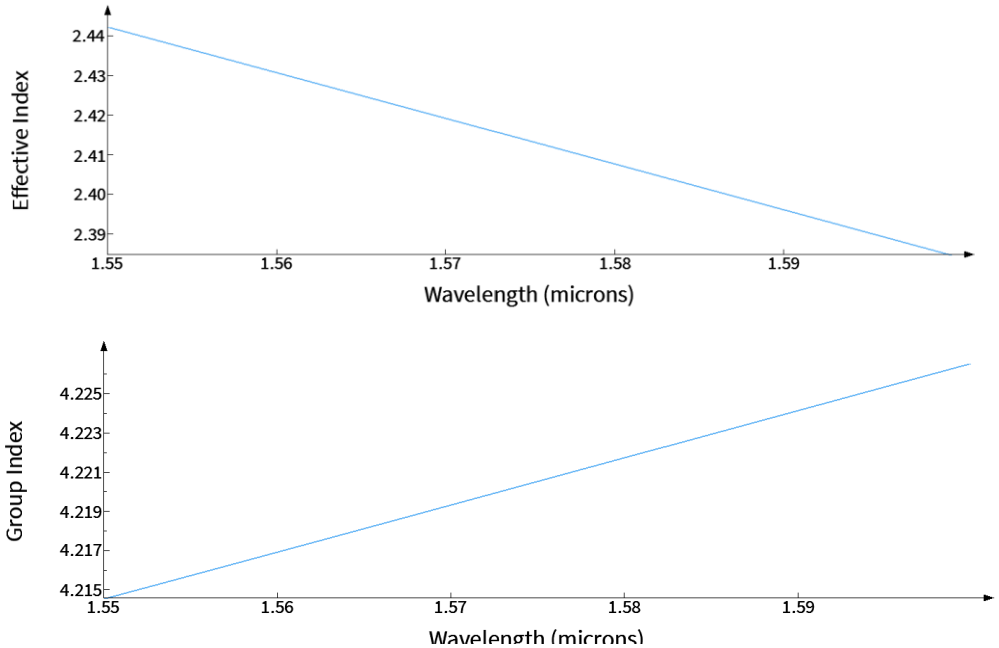

Figure 3: a) Effective index vs. wavelength (top), b) Group index vs. wavelength (bottom)

After obtaining the modal analysis data, effective index was fit with respect to the wavelength. Taylor expansion was used to model effective index with respect to the wavelength. The equation is.

$$n_{eff}[\lambda] = 2.44 + 1.127(\lambda - 1.55) + .033(\lambda - 1.55)^2 \quad (6)$$

3.2 *Layout*

The first design proposal of six layouts of unbalanced Mach-Zander interferometer was drawn on a grid of 610um * 405um using KLayout as shown in figure 4.

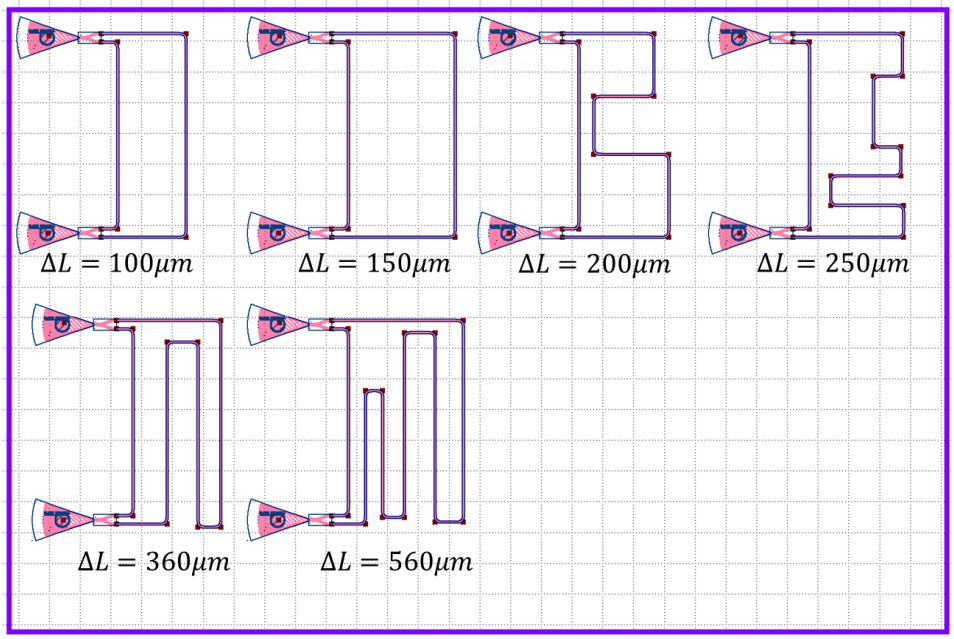

Figure 3: MZI layouts using KLayout.

Theoretically, the FSR could be calculated using equation 5. Table 2 provides calculated FSR value for different ΔL.

$\Delta L(\mu m)$	FSR (nm)
100.0	5.7
150.0	3.8
200.0	2.8
250.0	2.3
360.0	1.6
560.0	1.0

Figure 4 shows the simulated spectrum at different values of ΔL performed using INTERCONNECT.

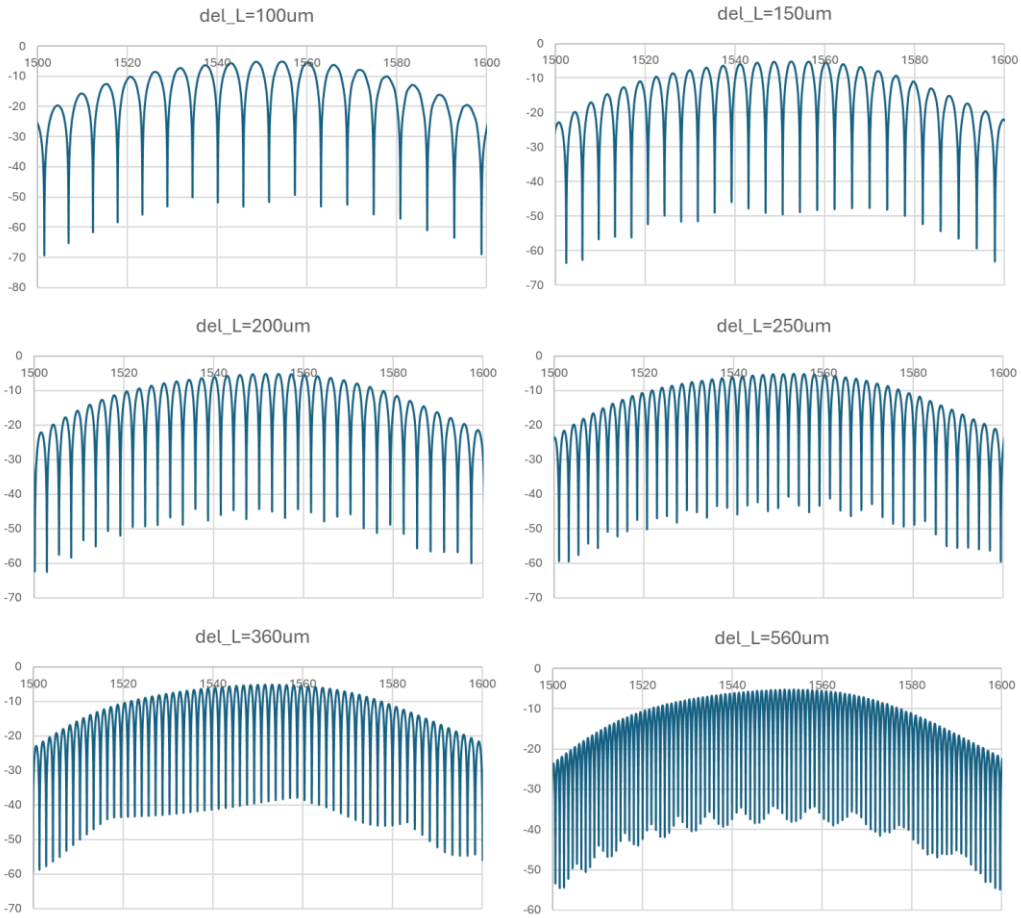

4. Manufacturing variability

It is often essential that the central wavelength or the Free spectral range of a photonic integrated circuit is fabricated to its requirement. Small errors caused due to manufacturing could often vary the performance of the circuit. These manufacturing errors could be due to variation in waveguide thickness, variation in the feature size, variation in material properties, etc. To study the variation of effective index and group index, corner analysis will be performed on the waveguide. Variation of FSR and central wavelength due to manufacturing errors on each circuit will be studies.

4.1 Corner analysis

In this section, the variation of effective index and the group index due to the variation in the size of waveguide is studied. A waveguide with a nominal size of 500*220nm was considered. The waveguide height varied between 215.3nm and 223.1nm, while the width varied from 470nm to 510nm. MODE simulations were performed to predict the group index and effective index at different corners and nominal waveguide size using corner method analysis. Figure 5 shows the nominal and corner dimensions of the waveguide. Figure 6a shows the variation of effective index and group index using corner analysis. The nominal effective index and group index is estimated to be 2.4491 and 4.2003, respectively. Due to the manufacturing errors of the waveguide, the effective index at 1550nm varies between 2.373 to 2.473, while the group

index varies between 4.173 to 4.255. Figure 7 shows the plot of effective index vs. wavelength due to manufacturing variation in the waveguide size.

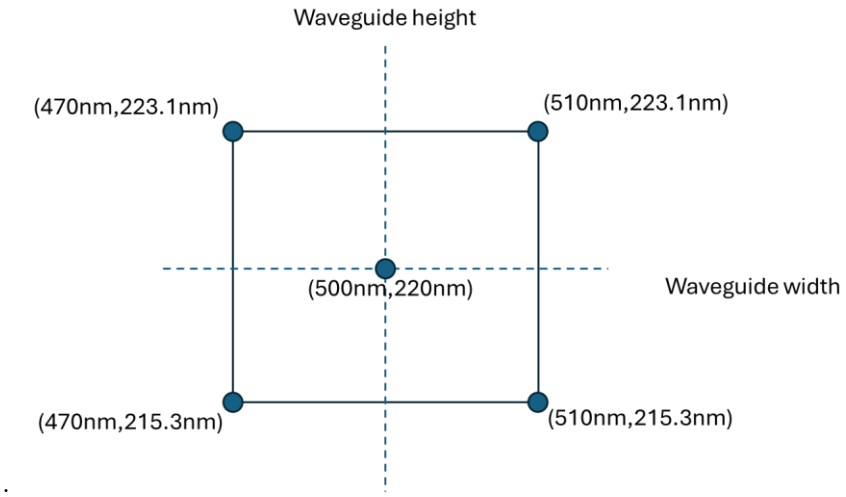

Figure 5: Variation of the waveguide's dimension

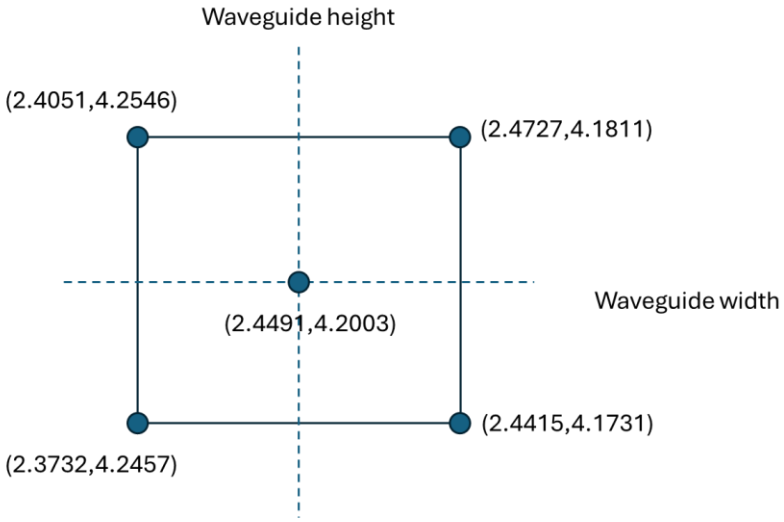

Figure 6: Variation of the refractive indices (effective index, group index) with variation in waveguide dimension.

Using frequency sweep in Lumerical MODE, the variation of effective index with wavelength was estimated. The data was exported and coefficients of Taylor expansion for compact model was estimated for different variations in the waveguide geometry. Coefficients n1, n2, n3 are listed in Table 3.

Waveguide geometry	n1	n2	n3
470nm x 215.3nm	2.373252	-1.20952	0.006278
470nm x 223.1nm	2.40508	-1.1944	-0.01631
510nm x 223.1nm	2.472669	-1.10231	-0.02525
510nm x 215.3nm	2.441515	-1.11745	-0.00972
500nm x 220nm	2.449097	-1.13016	-0.02107

Table 3: Compact model refractive index coefficients for different waveguide geometry

Based on Table 3, variation of effective index and group index is evaluated for different waveguide geometries as shown in figure 7.

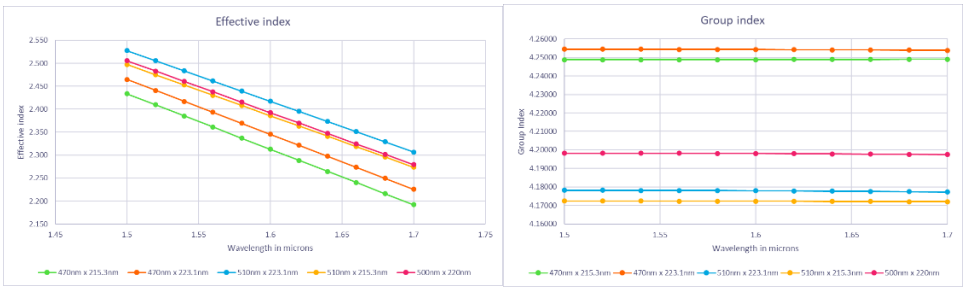

Figure 7: Effective index and group index vs. wavelength for different waveguide geometries

Based on the group index and the optical path difference as listed in table 2, variation in FSR is calculated in table 4.

	Free spectral range, FSR (nm)				
Optical path difference (microns)	470nm x 215.3nm	470nm x 223.1nm	510nm x 223.1nm	510nm x 215.3nm	500nm x 220nm
100	5.65	5.65	5.75	5.76	5.72
150	3.77	3.76	3.83	3.84	3.82
200	2.83	2.82	2.88	2.88	2.86
250	2.26	2.26	2.30	2.30	2.29
360	1.57	1.57	1.60	1.60	1.59
560	1.01	1.01	1.03	1.03	1.02

Table 4: Comparison of FSR for difference waveguide geometries at different OPD of the Mach-Zander Interferometers.

5. Fabrication

5.1. Fabrication process

Photonic devices were fabricated using the NanoSOI MPW process by Applied Nanotools Inc., which employs 100 keV electron beam lithography. The base material was 200 mm SOI wafers with a 220 nm device layer and 2 µm oxide buffer, pre-diced into 25×25 mm substrates. After cleaning with piranha solution, HSQ resist was spin-coated and patterned using a JEOL JBX-8100FS e-beam system at UBC, with proximity effect correction and optimized writing order. Post-exposure development used TMAH, followed by optical inspection. Chips were mounted

on a 4" handle wafer and etched via ICP-RIE using chlorine. Resist removal was done with a 10:1 buffer oxide wet etch, and SEM verified etch quality. A 2.2 µm oxide cladding was deposited by PECVD using TEOS at 300°C. Reflectometry confirmed layer thicknesses throughout the process before delivery.

To characterize the devices, a custom-built automated test setup [1, 5] with automated control software written in Python was used [2]. An Agilent 81600B tunable laser was used as the input source and Agilent 81635A optical power sensors as the output detectors. The wavelength was swept from 1500 to 1600 nm in 10 pm steps. Polarization maintaining (PM) fiber was used to maintain the polarization state of the light, to couple the TE polarization into the grating couplers [3]. A 90º rotation was used to inject light into the TM grating couplers [3]. Polarization maintaining fiber array was used to couple light in/out of the chip [4].

6. Experimental Results

Table 5 summarizes the results of both simulations and experiments for different structures with various cross sections, path length differences, and polarizations. The group indices and FSRs are found at 1.55 µm with waveguide geometry 500nm*220nm. There is a particularly good agreement between simulation and experimental results.

Table 5: Summary of simulation and experimental results for the MZI with different parameters

$\Delta L(\mu m)$	FSR (nm)	ng (simulated)	FSR (nm) experimental	ng (experimental)
100.0	5.7	4.2	5.8	4.244
150.0	3.8		3.85	4.195
200.0	2.8		2.84	4.179
250.0	2.3		2.296	4.184
360.0	1.6		1.59	4.193
560.0	1.0		1.02	4.19

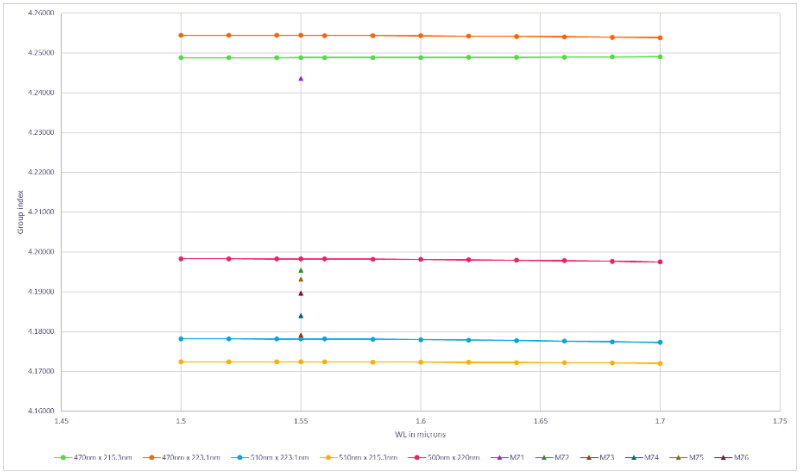

Figure 8: Group index extracted for measurement data different MZI at 1550nm (represented by triangle) at TE mode.

7. Acknowledgments

I acknowledge the edX UBCx Phot1x Silicon Photonics Design, Fabrication and Data Analysis course, which is supported by the Natural Sciences and Engineering Research Council of Canada (NSERC) Silicon Electronic-Photonic Integrated Circuits (SiEPIC) Program. The devices were fabricated by Cameron Horvath at Applied Nanotools, Inc. Omid Esmaeeli performed the measurements at The University of British Columbia. We acknowledge Lumerical Solutions, Inc., Mathworks, Mentor Graphics, Python, and KLayout for software design.

8. References:

[1] Lukas Chrostowski, Michael Hochberg, chapter 12 in "Silicon Photonics Design: From Devices to Systems", Cambridge University Press, 2015

[2] http://siepic.ubc.ca/probestation, using Python code developed by Michael Caverley.

[3] Yun Wang, Xu Wang, Jonas Flueckiger, Han Yun, Wei Shi, Richard Bojko, Nicolas A. F. Jaeger, Lukas Chrostowski, "Focusing sub-wavelength grating couplers with low back reflections for rapid prototyping of silicon photonic circuits", Optics Express Vol. 22, Issue 17, pp. 20652-20662 (2014) doi: 10.1364/OE.22.020652

[4] www.plcconnections.com, PLC Connections, Columbus OH, USA.

[5] http://mapleleafphotonics.com, Maple Leaf Photonics, Seattle WA, USA.